An Automated OCT-Based Glaucoma Detection with 3-D ResNet18 and a Convolutional Block Attention Module

Venkateswara Rao Kalidindi
Department of Artificial Intelligence and Machine Learning, Aditya University, Surampalem, Kakinada, Andhra Pradesh, India
kvrsnsg@gmail.com (corresponding author)

Harinadh Varikuti
Shri Vishnu Engineering College for Women, Bhimavaram, Andhra Pradesh, India
varikutiharinadh@gmail.com

Manikanta Kalyan Choppa
Department of Artificial Intelligence and Machine Learning, Aditya University, Surampalem, Kakinada, Andhra Pradesh, India
Manikantacm016@gmail.com

Priyanth Dunna
Department of Artificial Intelligence and Machine Learning, Aditya University, Surampalem, Kakinada, Andhra Pradesh, India
dunnapriyanth1@gmail.com

Venkat Rammohan Gummalla
Department of Artificial Intelligence and Machine Learning, Aditya University, Surampalem, Kakinada, Andhra Pradesh, India
ramu84kkd@gmail.com

Sireesha Malla
Department of Information Technology of Computer Applications, Andhra University, Visakhapatnam, Andhra Pradesh, India
mallasireesha72@gmail.com

Received: 16 September 2025 | Revised: 1 November 2025 | Accepted: 9 November 2025

DOI: https://doi.org/10.48084/etasr.14835

ABSTRACT

In this work, a Deep Learning (DL) technique utilizing a 3D ResNet18 model supplemented with a Convolutional Block Attention Module (CBAM) was proposed to successfully extract volumetric characteristics while prioritizing the most informative spatial areas for classification. The data comprised labeled Optical Coherence Tomography (OCT) volumes processed with normalization, resizing, augmentation, and balanced splitting to minimize data leakage. The experimental results indicated that the model obtained stable performance, with validation and test AUC values of 0.9640 and 0.9495, respectively, and corresponding accuracy rates of 87.88% and 85.59%. Additionally, a comparison with previous models further validated the effectiveness of the current model. These results confirm that the framework can reliably achieve high sensitivity and specificity in separating glaucoma from normal cases.

Keywords-OCT scans; glaucoma detection; 3D ResNet18; CBAM

I. INTRODUCTION

OCT is a non-invasive technique that enables the visualization of high-resolution cross-sectional retinal structures, allowing the detection of morphological changes that are not visible with traditional approaches [1]. OCT has become more advanced with its ultra-high-resolution version, which gives better scans and reduces time [2]. Additionally, the Anterior Segment OCT (AS-OCT) is utilized for the characterization of the anatomical structures and helps identify possible risk factors [3, 4].

Despite these advantages, the OCT imaging technique still has challenges. For example, manual evaluation by experts, while effective, is time-consuming, subjective, and prone to inter-observer variability. Moreover, OCT can capture only a part of the eye, causing a limited assessment. To prevent this limitation, OCT has been enhanced by a whole-eye imaging technique which enables the examination of the full ocular. As there are many complications regarding eye diseases, there is a need for early detection. The integration of Artificial Intelligence (AI) into ocular imaging can handle large amounts of data and plays a significant role in the diagnosis and management of ophthalmological diseases like glaucoma with high accuracy [5, 6].

Glaucoma is a neurodegenerative disease that results in irreversible blindness and vision loss due to the death of Retinal Ganglion Cells (RGCs). Although there are many clinical examinations for this, OCT imaging - particularly Spectral Domain OCT (SD-OCT) - is widely utilized for glaucoma diagnosis offering high accuracy [7]. Specifically, this method evaluates different parameters, which are crucial for glaucoma detection, like the Retinal Nerve Fiber Layer (RNFL) thickness, macular parameters, and Optic Nerve Head (ONH) morphology. DL techniques, such as 2D and 3D Convolutional Neural Networks (CNNs), may directly learn the features from OCT images. 2D CNNs are able to process B-scans and make predictions of the volume, while 3D CNNs are capable of capturing spatial context directly from the volumetric OCT data [8]. The OCT imaging approach has the ability to visualize Aqueous Humor Outflow (AHO), providing valuable insights for monitoring Intraocular Pressure (IOP) regulation, and serves as an effective therapeutic intervention [9].

Various ML and image processing models have been applied to detect glaucoma through OCT images, including CNNs, Recurrent Neural Networks (RNNs), as well as self-organizing maps for automated feature extraction and classification of OCT scans. Ensemble learning approaches, residual networks, and Fully Convolutional Networks (FCNs) have presented excellent performance in glaucoma detection. Additionally, segmentation-based techniques, such as superpixel classification, thresholding, edge-based segmentation, and fuzzy morphological algorithms, have been adopted. Furthermore, advanced customized models, like Inception-v3 and ResNet, have been evaluated on publicly available OCT datasets, enabling the automatic detection of glaucoma. All these computational approaches represent a wide range of frameworks that aim at enhancing automated glaucoma detection [10, 11].

Authors in [12] evaluated several DL models in order to improve the proposed model's accuracy and demonstrated that their proposed method achieved better performance in both classification and segmentation of brain tumors. In [13], a 3D computational microscopy framework called Optical Coherence Refraction Tomography (OCRT) was investigated. The physics-based model utilized refraction-aware iterative reconstruction algorithms to accurately recover volumetric tissue structures. Synthesized as well as biological datasets were evaluated, achieving higher resolution 3D reconstructions and reduced artifacts, indicating the advanced imaging capabilities of OCRT. Similarly, authors in [14] devised a non-invasive, label-free 3D Doppler-OCT (D-OCT) method for tumor spheroid detection. This dynamic contrast algorithm exploited temporal speckle changes to visualize cellular activity and subsequent tissue microstructural changes while maintaining spatial and temporal resolution.

In [15], a 3D CNN framework was proposed, driven by attention to detect glaucoma from 3D volumetric OCT images. This approach drew attention over relevant portions of the retina and increased the analysis of the relationship between structure and function. It was tested on datasets containing healthy retinas and retinas that were diagnosed with glaucoma, with the results revealing improved eye health diagnosis and stronger structure-function correlations compared to conventional measures. Additionally, authors in [16] incorporated sequential 2D OCT scans into volumetric 3D images, enabling depth-resolved reflectivity profiles from both human retina and skin to provide microstructural information. Following that, in [17], a novel 3D SD-OCT method was utilized for the detection of fluid-filled regions in the macula. The authors quantified retinal texture and applied classification algorithms that had been validated on datasets of patients. The goal was to provide a better diagnostic accuracy compared to the standard method of 2D analysis.

A technique for automated segmentation of the optic disc in 3D OCT images was utilized in [18], incorporating geometric constraints and image intensity characteristics. An accurate delineation of optic disc boundaries was based on segmentation results from a graph and was validated using expert annotations on glaucoma and healthy datasets. Similarly, a 3D spectral OCT retinal vessel segmentation methodology was applied in [19], employing intensity, gradient, and structural features. The results revealed effective vessel extraction and generated detailed 3D vascular maps from the scans based on human retina imaging, demonstrating an accurate volumetric analysis of retinal structures obtained from OCT data. Authors in [20] introduced a 3D OCT synthetic data generation method using Active Shape Models that preserve the statistical and textural properties of real-world datasets, even in cases of diabetic macular edema, with the aim of providing benchmarks and augmentation for deep learning. Apart from these, a motion correction framework was created based on optimized image registration and orthogonal scans that reduced errors in retinal thickness and vascular mapping in healthy and glaucomatous eyes [21]. Similarly, in [22], a two-stage thin-plate spline correction for axial artifacts in SD-OCT scans was introduced, significantly increasing the accuracy of 3D retinal reconstructions and alignments with reference surfaces.

Authors in [23] developed a lightweight CNN model for the detection of macular edema in OCT images. Deep OCT used prior analysis, including BM3D denoising, flattening retinal layers, and cropping to achieve strong performance metrics and generate feature activation maps that outline potential areas of pathology. A forward-looking resonant fiber-optic endoscope was examined in [24] for fast retina 3D imaging, containing advanced imaging capabilities, such as resonant scanning frequencies, providing the user the opportunity to select, and imaging the tissue in real-time at 40 kHz with swept-source OCT. Improvements in resolution, speed, and penetration were highlighted in [25] through the use of broad-bandwidth light sources and fast-speed detection, which allowed for deeper retinal and choroidal visualization with less motion artifacts throughout 3D OCT.

Beyond biomedical applications, authors in [26] demonstrated the use of OCT in art conservation by employing en-face systems at 850 nm and 1300 nm to non-invasively image paintings. High-resolution B- and C-scans revealed varnish, paint layers, and under-drawings that would allow conservators to view preparatory layers without damaging the paintings. In [27], a deep ensemble CNN capable of automating the segmentation of all three retinal fluid types in OCT images was presented. It was evaluated on the RETOUCH dataset, effectively segmenting cysts (fluid) in pathologies, such as macular edema and age-related macular, while it also outperformed prior methods with an increase in overall accuracy of 1.8%. Finally, authors in [28] developed a non-rigid 3D motion correction framework for OCT angiography, able to align axial layers and vascular features, which was robust even in pathological cases.

Studies on 3D OCT imaging for disease detection provide valuable insights into the rapid advancements of imaging systems, computational algorithms, and DL frameworks. However, several research gaps remain. A major limitation is the usage of small, disease-specific or synthetic datasets, causing issues of data imbalance, less generalization, and reduced clinical applicability. Additionally, while computational imaging models and high-speed OCT hardware have improved resolution and acquisition speed, their high cost and computational requirements restrict real-time deployment in clinical practice. To address these challenges, the current study presents a DL framework using a 3D ResNet-18 architecture to capture spatiotemporal and volumetric features from OCT data. The network was further enhanced by the integration of Convolutional Block Attention Module (CBAM) and a classification head was utilized to map the extracted representations for glaucoma detection.

II. METHODOLOGY

A. *Dataset Description*

This study employed 3D OCT volumes, which were saved in .npy format. Each file corresponded to a single OCT volume with the labels "Normal" or "Glaucoma". "Normal" represents a retinal structure that is healthy, while scans from patients diagnosed with glaucoma belonged to the "Glaucoma" class. Data leakage was prevented by incorporating a patient identifier in every filename, which ensured that all scans from the same patient appear only in one subset. The dataset was divided as a patient-wise split: 80% train, 14% test, and 6% validation. This division ensured that the model was evaluated on completely unseen patients. This led to an imbalance in the dataset since normal and glaucoma cases were not equally distributed. For this reason, augmentation and minority class oversampling was applied to balance the sample size of training data [29].

B. *Pre-Processing*

OCT scans were preprocessed to make the data clean, uniform, and ready for training. Each scan was normalized by scaling its pixel values to the range [0, 1], which made training more stable and prevented calculation errors. All scans were then resized to 1 × 64 × 64 × 128 using interpolation, since the original scans had different dimensions. To improve robustness against variability in imaging conditions and patient anatomy, data augmentation was applied on the training set using the TorchIO library. This included random affine transformations (scale factor 0.9 - 1.1 and rotations up to ± 10°) to simulate geometric variability, random flips along spatial axes to mimic mirrored anatomy, and random Gaussian noise was added to the scans to imitate the type of noise that usually appears during the image capturing process.

C. *Proposed Model*

Figure 1 illustrates the proposed model, which combines a 3D ResNet18 backbone with a CBAM, to classify glaucoma from OCT volumes. Next, a preprocessed 1 × 64 × 64 × 128 OCT scan was taken, with the three axes indicating the retinal volume and the single channel showing grayscale intensity. The model started with a 3D convolutional preprocessing block using sequential normalization, ReLU configuration, and a 7 × 7 × 7 kernel with stride 2 and padding 3, followed by a max-pooling layer, while keeping important spatial features that reduce the size.

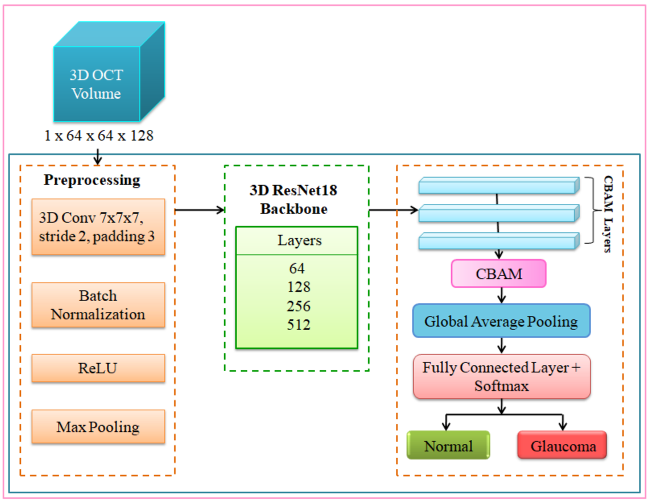

Fig. 1. Proposed architecture of 3D RCBAM.

The main feature extraction was performed using the 3D ResNet18 backbone, which contains four residual stages with increasing filter sizes (64, 128, 256, and 512) and skip connections that help secure the information. After feature extraction, the CBAM module used channel attention and spatial attention to identify the most important areas and patterns in the OCT images that are related to glaucoma. The refined features were then passed through a Global Average Pooling (GAP) layer to create a 512-dimensional vector of attributes that was supplied to a Fully Connected (FC) layer and had a SoftMax activation to classify the input. The model was trained with an optimization process that updates weights to reduce classification errors, allowing it to effectively capture both large and small details in the scans while focusing on the areas that are most important to glaucoma detection.

D. 3D ResNet18

Figure 2 depicts the 3D ResNet18 model adapted from the standard 2D ResNet18 designed for medical imaging tasks such as OCT scans. The 3D ResNet18 uses three-dimensional convolutions that also store features across height, width, and depth, securing volumetric historical data compared to the 2D version. The input was an OCT volume represented as a tensor of dimensions 1 × 64 × 64 × 128 (channels × depth × height × width), which was reduced, creating a feature model with a size of 64 × 32 × 32 × 64. The network started with an initial convolutional block based on a 7 × 7 ×7 3D convolution with stride 2.

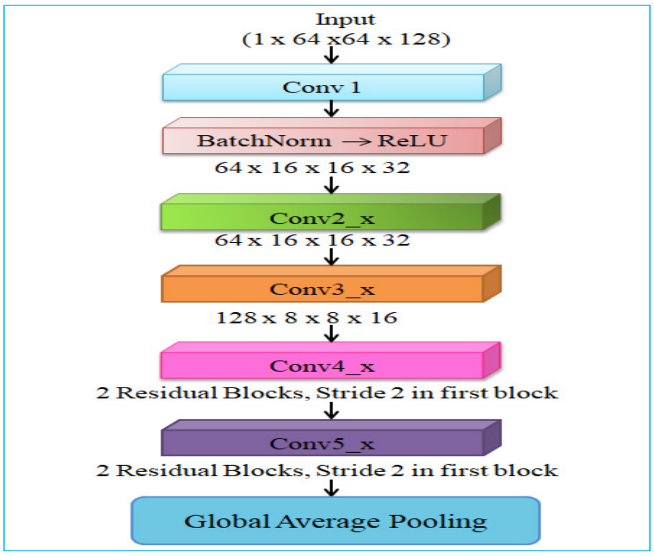

Fig. 2. 3D ResNet18 model.

The core of the network was organized into four residual stages, each containing multiple residual units. A residual unit consisted of two 3 × 3 × 3 convolutional layers, each followed by batch normalization and ReLU activation. ResNet is defined by its use of unique skip connections, which help the input of a block, *x*, to bypass the convolutional layers and connect right to the output of the residual layer. The process of transformation can be defined mathematically as:

$$y = f(x, w) + x \tag{1}$$

where *f(x, w)* represents the residual mapping learned by the convolutional layers with weights *w*, and *y* is the output of the block.

By addressing the issue of vanishing gradients, this approach made it simpler to train more complex networks quickly. Conv1 generated 64 feature maps of size 32 × 32 × 64, Conv2_x kept 64 feature maps, Conv3_x grew to 128 feature maps, Conv4_x grew to 256 feature maps, and Conv5_x generated 512 feature maps. Following the last residual stage, the 3D feature maps were reduced into a small vector structure using GAP, giving a 512-dimensional feature vector. The 3D ResNet18 utilized this vector as the high-level volumetric feature.

E. CBAM

CBAM was placed after the ResNet backbone, to strengthen the extracted features. The mechanism worked in two stages: channel attention followed by spatial attention (Figure 3). The Channel Attention Module (CAM) focused on identifying the most informative feature channels. For an input feature map $F \in R^{C \times H \times W \times D}$, both GAP and global max pooling were performed along the spatial axes. The resulting descriptors were then passed through a shared Multilayer Perceptron (MLP), their responses were merged using element-wise addition, and a sigmoid function was applied to obtain the channel attention map.

$$M_c(F) = \sigma\begin{pmatrix} MLP(AvgPool(F)) \\ +MLP\,(MaxPool(F)) \end{pmatrix} \tag{2}$$

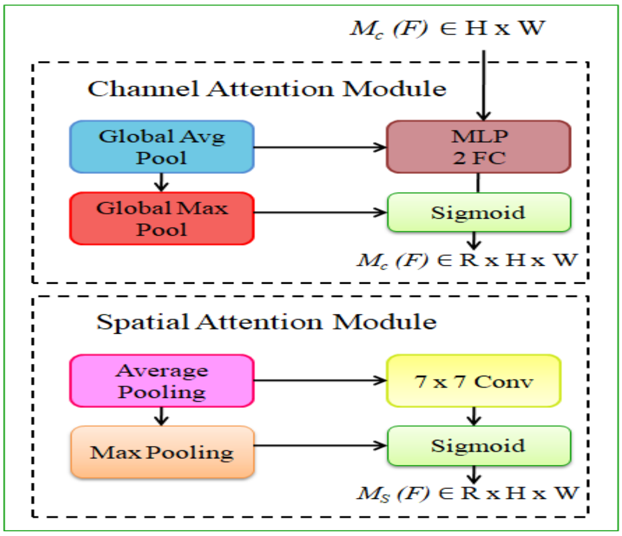

Fig. 3. CBAM model.

This process reduced the influence of less relevant channels while emphasizing the most significant ones. After this, Spatial Attention Module (SAM) highlighted the important regions within the feature maps. To achieve this, the average-pooled and max-pooled maps were merged and then processed through a 7 × 7 convolution layer. A sigmoid function was used to create the spatial attention map:

$$M_s(F) = \sigma\big(f_{7\times7}([AvgPool(F); MaxPool(F)])\big) \tag{3}$$

where $f_{7\times7}$ is the convolution operation and [;] means concatenation along the channel axis. The refined feature map was obtained by combining both channel and spatial attention outputs:

$$F' = M_s(M_c(F) \otimes F) \otimes (M_c(F) \otimes F) \quad (4)$$

where $\otimes$ denotes element-wise multiplication.

In order to identify less abnormal changes in OCT areas, CBAM ensured that the network chose specific retinal tissues while minimizing the effect of background or duplicate data.

F. Classification Head

The CBAM was used to change the features when the network output was converted into a 512-dimensional vector format. In an FC layer, the two output neurons indicated normal and glaucoma cases. These logits were turned into useful probabilities using a softmax activation function. The definition of the probability pattern over the two classes is:

$$P\,(y \mid x) \;=\; \frac{e^{z_i}}{\sum_{j=1}^{2} e^{z_j}} \quad (5)$$

where z_i denotes the logit that comes with the i-th class. Adding the exponential values of each logit, the factor of two ensures that the output probabilities are equal and lies between 0 and 1. The class with the higher probability will be used to make the final prediction. After mapping new features identified from OCT scans, this classification head also helps with accurate glaucoma detection.

III. RESULTS AND ANALYSIS

The proposed model demonstrated strong performance in detecting glaucoma, as presented in Table I. The model achieved an AUC of 0.9640 on validation and an AUC of 0.9495 on testing. The AUC metric indicates the capability in classification between normal and glaucoma classes. AUC values close to 1.0 indicate high-quality classification outputs. Accuracy was used to determine the proportion of correctly classified samples among all cases, while the F1-score provided a balance between how many predicted positive cases were actually positive (Precision) and how many actual positive cases were correctly predicted (Recall).

TABLE I. CLASSIFICATION METRICS FOR VALIDATION AND TESTING SAMPLES

Metric	**Val (mean ± std)**	**Test (mean ± std)**
AUC	0.9640 ± 0.015	0.9495 ± 0.036
F1-score	0.7600 ± 0.018	0.7460 ± 0.046
Accuracy	0.8788 ± 0.020	0.8559 ± 0.040

The results illustrated in Table I are presented as mean ± std, where the mean is the average value of runs and the standard deviation shows how much the results changed between runs. The accuracy was 0.8788 ± 0.020 on validation and 0.8559 ± 0.040 on testing, which is a good overall correctness. The F1-score was 0.7600 ± 0.018 on validation and 0.7460 ± 0.046 on testing. Overall, these results indicated that the model is accurate, stable, and reliable, with some changes between runs.

Figure 4 illustrates the confusion matrices of both the validation and testing samples. The predicted class is shown on the x-axis in both images, while the actual class is given on the y-axis. In Figure 4(a), the model correctly classified 19 Normal and 68 Glaucoma samples. However, it misclassified 3 Normal samples as Glaucoma and 9 Glaucoma samples as Normal, giving a total of 99 validation samples. In Figure 4(b), the model correctly classified 47 Normal and 143 Glaucoma cases, while it misclassified 6 Normal images as Glaucoma and 26 Glaucoma images as Normal, resulting in a total of 222 test images. From these results, it is clear that most cases were along the correct predictions.

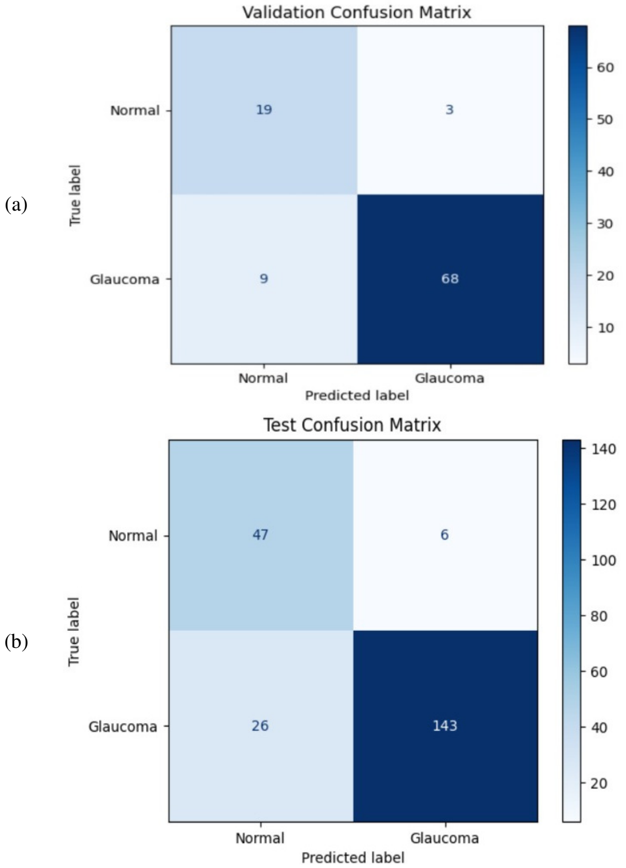

Fig. 4. Confusion matrices for: (a) validation and (b) test samples.

To further validate these findings, a comparison of the proposed model with previous OCT models is presented in Table II.

TABLE II. AUC COMPARISON OF PROPOSED MODEL WITH EXISTING OCT-BASED GLAUCOMA DETECTION METHODS

Model	**AUC value**
2D-ResNet18 (ONH-OCT) [8]	0.943
3D-DenseNet121 [8]	0.960
AG-OCT [15]	0.938
3D-ResNet18 + CBAM (proposed)	0.9640

The comparative analysis demonstrated that the proposed 3D-ResNet18 model with a CBAM provided enhanced capabilities in automated glaucoma assessment based on OCT data. Previous studies utilizing 3D-CNN-based approaches to detect glaucoma from OCT data noted AUC values ranging from 0.938 to 0.96. The proposed model provided greater evidence of discrimination abilities, reporting a 0.9640 AUC on the validation set and a 0.9495 AUC on the testing set. This improvement reveals that the model took advantage of volumetric information and attention-based feature refinement to increase sensitivity to subtle changes in the structure associated with the disease of glaucoma.

IV. CONCLUSION

This study combined a 3D ResNet18 model with the Convolutional Block Attention Module (CBAM) to classify glaucoma from volumetric Optical Coherence Tomography (OCT) scans. The results demonstrated strong performance achieving a validation AUC of 0.9640 and a testing AUC of 0.9495, as well as high accuracy and F1-score values. The confusion matrices on both validation and testing datasets confirmed that the model could effectively separate the two classes, with a small number of misclassifications. A comparison with previous models further validated that the proposed model offers a more reliable and accurate solution for glaucoma detection.

Future work should focus on training the model with bigger and more varied datasets collected from different devices and different groups of patients. This will make it more general and reliable. Using this framework in real-time clinics and hospitals with easy-to-use interfaces can help doctors check OCT scans more quickly and make faster decisions. The diagnosis can become more accurate if the OCT scan results are combined with other medical information, such as patient history or genetic data.

REFERENCES

[1] A. N. Kuo, R. P. McNabb, and J. A. Izatt, "Advances in Whole-Eye Optical Coherence Tomography Imaging," *Asia-Pacific Journal of Ophthalmology*, vol. 8, no. 2, pp. 99–104, Mar. 2019, https://doi.org/10.22608/APO.201901.

[2] K. C. Shih, R. H.-K. Tse, Y. T.-Y. Lau, and T. C.-Y. Chan, "Advances in Corneal Imaging: Current Applications and Beyond," *The Asia-Pacific Journal of Ophthalmology*, vol. 8, no. 2, Mar. 2019, Art. no. 105, https://doi.org/10.22608/APO.2018537.

[3] R. N. Weinreb and S. Moghimi, "Advances in Ocular Imaging," *The Asia-Pacific Journal of Ophthalmology*, vol. 8, no. 2, Mar. 2019, Art. no. 97, https://doi.org/10.22608/APO.201984.

[4] J. Shan, C. DeBoer, and B. Y. Xu, "Anterior Segment Optical Coherence Tomography: Applications for Clinical Care and Scientific Research,""*Asia-Pacific Journal of Ophthalmology*, vol. 8, no. 2, pp. 146–157, Mar. 2019, https://doi.org/10.22608/APO.201910.

[5] R. Kapoor, B. T. Whigham, and L. A. Al-Aswad, "Artificial Intelligence and Optical Coherence Tomography Imaging," *Asia-Pacific Journal of Ophthalmology*, vol. 8, no. 2, pp. 187–194, Mar. 2019, https://doi.org/10.22608/APO.201904.

[6] C. Y. Cheung, F. Tang, D. S. W. Ting, G. S. W. Tan, and T. Y. Wong, "Artificial Intelligence in Diabetic Eye Disease Screening," *Asia-Pacific Journal of Ophthalmology*, vol. 8, no. 2, pp. 158–164, Mar. 2019, https://doi.org/10.22608/APO.201976.

[7] A. Ha and K. H. Park, "Optical Coherence Tomography for the Diagnosis and Monitoring of Glaucoma," *Asia-Pacific Journal of Ophthalmology*, vol. 8, no. 2, pp. 135–145, Mar. 2019, https://doi.org/10.22608/APO.201902.

[8] R. K. Rasel, F. Wu, M. Chiariglione, S. S. Choi, N. Doble, and X. R. Gao, "Assessing the efficacy of 2D and 3D CNN algorithms in OCT-based glaucoma detection," *Scientific Reports*, vol. 14, no. 1, May 2024, Art. no. 11758, https://doi.org/10.1038/s41598-024-62411-6.

[9] X. Xie, G. Akiyama, T. Bogarin, S. Saraswathy, and A. S. Huang, "Visual Assessment of Aqueous Humor Outflow," *Asia-Pacific Journal of Ophthalmology*, vol. 8, no. 2, pp. 126–134, Mar. 2019, https://doi.org/10.22608/APO.201911.

[10] A. Shabbir *et al.*, "Detection of glaucoma using retinal fundus images: A comprehensive review," *Mathematical Biosciences and Engineering*, vol. 18, no. 3, pp. 2033–2076, Mar. 2021, https://doi.org/10.3934/mbe.2021106.

[11] M. Ashtari-Majlan, M. M. Dehshibi, and D. Masip, "Deep Learning and Computer Vision for Glaucoma Detection: A Review." arXiv, July 31, 2023, https://doi.org/10.48550/arXiv.2307.16528.

[12] P. Murala and K. N. Rao, "Multi-Class Brain Tumor Diagnosis Using a Vision Transformer with MRI Image Segmentation," *Engineering, Technology & Applied Science Research*, vol. 15, no. 4, pp. 26120–26127, Aug. 2025, https://doi.org/10.48084/etasr.11592.

[13] K. C. Zhou *et al.*, "Computational 3D microscopy with optical coherence refraction tomography," *Optica*, vol. 9, no. 6, pp. 593–601, 2022.

[14] I. A. El-Sadek *et al.*, "Three-dimensional dynamics optical coherence tomography for tumor spheroid evaluation," *Biomedical optics express*, vol. 12, no. 11, pp. 6844–6863, 2021.

[15] Y. George, B. J. Antony, H. Ishikawa, G. Wollstein, J. S. Schuman, and R. Garnavi, "Attention-Guided 3D-CNN Framework for Glaucoma Detection and Structural-Functional Association Using Volumetric Images," *IEEE Journal of Biomedical and Health Informatics*, vol. 24, no. 12, pp. 3421–3430, Dec. 2020, https://doi.org/10.1109/JBHI.2020.3001019.

[16] A. G. Podoleanu, J. A. Rogers, D. A. Jackson, and S. Dunne, "Three dimensional OCT images from retina and skin," *Optics Express*, vol. 7, no. 9, pp. 292–298, 2000.

[17] G. Quellec, K. Lee, M. Dolejsi, M. K. Garvin, M. D. Abramoff, and M. Sonka, "Three-Dimensional Analysis of Retinal Layer Texture: Identification of Fluid-Filled Regions in SD-OCT of the Macula," *IEEE Transactions on Medical Imaging*, vol. 29, no. 6, pp. 1321–1330, June 2010, https://doi.org/10.1109/TMI.2010.2047023.

[18] K. Lee, M. Niemeijer, M. K. Garvin, Y. H. Kwon, M. Sonka, and M. D. Abramoff, "Segmentation of the Optic Disc in 3-D OCT Scans of the Optic Nerve Head," *IEEE Transactions on Medical Imaging*, vol. 29, no. 1, pp. 159–168, Jan. 2010, https://doi.org/10.1109/TMI.2009.2031324.

[19] M. Niemeijer, M. K. Garvin, B. van Ginneken, M. Sonka, and M. D. Abràmoff, "Vessel segmentation in 3D spectral OCT scans of the retina," *in Medical Imaging*, San Diego, CA, USA, 2008, https://doi.org/10.1117/12.772680.

[20] H. Danesh, K. Maghooli, A. Dehghani, and R. Kafieh, "Synthetic OCT data in challenging conditions: three-dimensional OCT and presence of abnormalities," *Medical & Biological Engineering & Computing*, vol. 60, no. 1, pp. 189–203, 2022, https://doi.org/10.1007/s11517-021-02469-w.

[21] M. F. Kraus *et al.*, "Quantitative 3D-OCT motion correction with tilt and illumination correction, robust similarity measure and regularization," *Biomedical optics express*, vol. 5, no. 8, pp. 2591–2613, 2014.

[22] B. Antony *et al.*, "Automated 3-D method for the correction of axial artifacts in spectral-domain optical coherence tomography images," *Biomedical optics express*, vol. 2, no. 8, pp. 2403–2416, 2011.

[23] G. Altan, "DeepOCT: An explainable deep learning architecture to analyze macular edema on OCT images," *Engineering Science and Technology, an International Journal*, vol. 34, Oct. 2022, Art. no. 101091, https://doi.org/10.1016/j.jestch.2021.101091.

[24] L. Huo, J. Xi, Y. Wu, and X. Li, "Forward-viewing resonant fiber-optic scanning endoscope of appropriate scanning speed for 3D OCT imaging," *Optics express*, vol. 18, no. 14, pp. 14375–14384, 2010.

[25] B. Považay *et al.*, "Impact of enhanced resolution, speed and penetration on three-dimensional retinal optical coherence tomography," *Optics Express*, vol. 17, no. 5, pp. 4134–4150, 2009.

[26] H. Liang *et al.*, "En-face optical coherence tomography-a novel application of non-invasive imaging to art conservation," *Optics Express*, vol. 13, no. 16, pp. 6133–6144, 2005.

[27] M. Rahil, B. N. Anoop, G. N. Girish, A. R. Kothari, S. G. Koolagudi, and J. Rajan, "A Deep Ensemble Learning-Based CNN Architecture for Multiclass Retinal Fluid Segmentation in OCT Images," *IEEE Access*, vol. 11, pp. 17241–17251, Feb. 2023, https://doi.org/10.1109/ACCESS.2023.3244922.

[28] S. B. Ploner *et al.*, "Efficient and high accuracy 3-D OCT angiography motion correction in pathology," *Biomedical Optics Express*, vol. 12, no. 1, pp. 125–146, 2020.

[29] *Glaucoma Detection Dataset*, https://www.kaggle.com/datasets/teamincribo/glaucoma-detection-dataset.